MODELLING HYDROTHERMAL FLUID FLOW IN A HIGH ANDEAN SETTING

John O'Sullivan[1], Ariel Vidal[1], Gonzalo Yáñez[3] and Jose Muñoz[2]

[1]Department of Engineering Science, University of Auckland, Private Bag 92019, Auckland 1142, New Zealand

[2]Departamento de Ingeniería Hidráulica y Ambiental, Universidad Católica de Chile, Vicuña Mackenna 4860, Santiago, Chile

[3]Departamento de Ingeniería Estructural y Geotecnia, Universidad Católica de Chile, Vicuña Mackenna 4860, Santiago, Chile

jp.osullivan@auckland.ac.nz

Keywords: *Geothermal, Andes, Pampa Lirima, TOUGH2, Reservoir modelling.*

ABSTRACT

Northern Chile (17-28°S) is located in a very suitable tectono-magmatic setting for the development of geothermal energy. It is composed of a volcanic chain associated with the active Nazca-South America plate boundary and quaternary volcanism is found along the high Andes and Altiplano, over a thick crust (~60 km), with climatic conditions ranging from arid to hyper arid. The hot fluids at shallow crustal levels in this region contribute to estimated geothermal resources in Chile in the order of 16000 MW (Lahsen *et al*. 2010).

A preliminary TOUGH2 model has been developed for the Pampa Lirima basin, which is one of the characteristic hydrothermal systems in the Northern Andean region. Data from geological, geophysical and geochemical studies of the area were combined to develop a conceptual model of the system which was then implemented as a numerical model in TOUGH2. Care was taken to accurately represent the high altitude and the low level of meteoric recharge. The locations and flow rates of surface features were used to calibrate the model to ensure that the position of the unsaturated zone above the water table and the flow balance in the basin agree with observations. Temperatures recorded in the springs and estimated from geochemistry were used to carry out a preliminary calibration of the subsurface.

The natural state model results agree well with the available data and suggest that the Pampa Lirima system is structurally controlled with a number of faults interacting to provide mechanisms for both upflow and recharge. Numerical experiments with the model also revealed that it is unlikely that a large steam zone exists within the system unless the reservoir temperatures exceed estimates obtained through geochemistry.

The insights gained into the Pampa Lirima system demonstrate the usefulness of developing numerical models at an early stage, even prior to the availability of exploration well data.

1. INTRODUCTION

The Andean Central Volcanic Zone in Northern Chile contains a number of active or potentially active volcanic systems (Tassi *et al*., 2010), many of them associated with geothermal systems. The Pampa Lirima basin approximately 1700 km north of Santiago contains one of these geothermal systems and in 2009 the Chilean geothermal company Energia Andina obtained the exploration concession for the area (Arcos *et al*., 2011). Since that time Energia Andina has developed an extensive surface exploration programme and gathered a significant amount of data.

The objective of the present study was the development of a preliminary numerical model of the Pampa Lirima basin, as a representative case study of high Andean hydrothermal systems. Available surface and subsurface data were used to develop the conceptual model and to calibrate the numerical model. The model has proven to be a useful tool for improving understanding of the Pampa Lirima system and may be useful in planning its development. As more data becomes available the model can be refined and calibrated further for use as a tool for investigating future production scenarios.

In the following subsections the available data are described and discussed. In Section 2 the model design is described and in Section 3 some preliminary results are presented.

1.1 Geology of the Pampa Lirima basin

The geology of the Pampa Lirima basin and its surroundings is characterised by a Mesozoic basement covered by volcanic and sedimentary rocks of Miocene age and Miocene to Pleistocene volcanic edifices (Figure 2a). No recent volcanic activity has been documented in the area. The Mesozoic basement comprises a fold and thrust belt of clastic-carbonate sequence underlying a volcanic sequence (Arcos *et al*., 2011). The Oligocene to Miocene formations consist of pyroclastic flows interbedded with sedimentary units, reaching a total thickness of 700 m. These units are partially covered by Miocene to Pleistocene volcanic edifices and their related products. The Oligo-Miocene rocks shows a structural style characterized by a succession of anticlinal and synclinal folds interpreted as the surface expression of a strike slip dextral fault (Arcos *et al*., 2011). A series of alignments and inferred faults can be recognized, trending NS, NW and NE (Figure 2a).

Hydrothermal alteration is most strongly developed close to the Lirima and San Andrés hot springs. In both areas the alteration processes have similar features, with a mineralogy assembly ranging from argillic to advanced argillic with presence of illite-smectite, illite-sericite to silica, alunite and kaolinite, which represents an acid-sulfate, locally steam-heated epithermal system. Previous descriptions of the area, together with the structural arrangement, inferred subsurface development and preliminary hydrogeochemical aspects, suggest that the Lirima and San Andrés hot springs are associated with a single hydrothermal system (Arcos *et al*., 2011).

1.2 Geophysics

Various geophysical surveys have been carried out in the zone and several results from them are reproduced in Section 2 (Arcos *et al*., 2011; Legault *et al*., 2012). A reduced-to-the-pole sub-product of the aeromagnetic survey reveals a high intensity anomaly in the northern sector related to Miocene-Pliocene volcanic activity. Also an apparently demagnetized zone can be recognized in the area

of the Lirima springs and there is a clear NS magnetic lineament coincident with regional structural trends. Additionally, a small network of seismic stations, installed over a six months period, recorded 3571 events (Arcos *et al*., 2011). It is interesting to note that some of the seismic events are aligned along the lineament captured by the aeromagnetic data thus reinforcing the idea of a major structural control within the area.

Magnetotelluric (MT) data reveals a shallow conductive layer (Figures 3a and 4a), interrupted in the centre by a higher resistivity zone. Considering the geothermal context, the south-west part of this conductivity anomaly could be interpreted as the clay cap of the geothermal reservoir (Arcos *et al*., 2011). The central resistive zone is worth noting as it coincides with the regional alignment previously discussed and inferred by different methodologies. A very distinctive conductive anomaly can be observed in the left part of Figures 3a and 4a. The geometry of this conductive anomaly suggests a massive body, with deep roots, but no geological or geophysical data is available to explain the nature of this anomaly.

Legault *et al*. (2012) presented results of a ZTEM airborne FMAG survey conducted over the Pampa Lirima area. The results, to some extent, correlate with the previous geophysical surveys and geology, showing fault structures and lithological contacts, as well as a prominent NE trending conductivity high over the Lirima hot spring field extending to San Andrés hot springs area (Figure 1d), which is consistent with the strong argillic alteration. However, the ZTEM results were not able to corroborate the major MT conductivity high below Pampa Lirima springs (Legault *et al*. 2012). This inconsistency may be attributed to the much lower penetration depth capabilities of the ZTEM methodology compared to the MT experiments.

a)

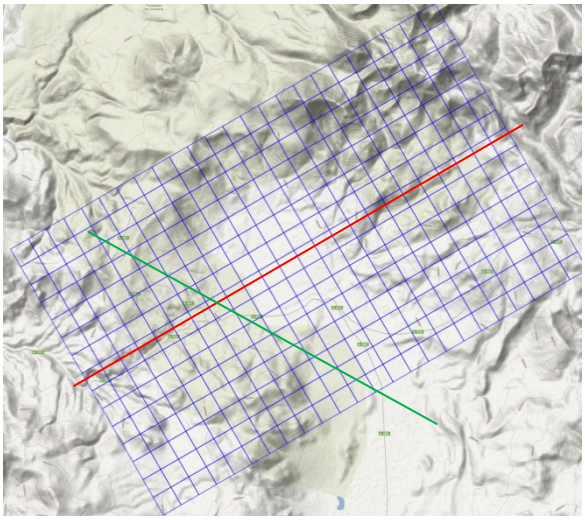

b)

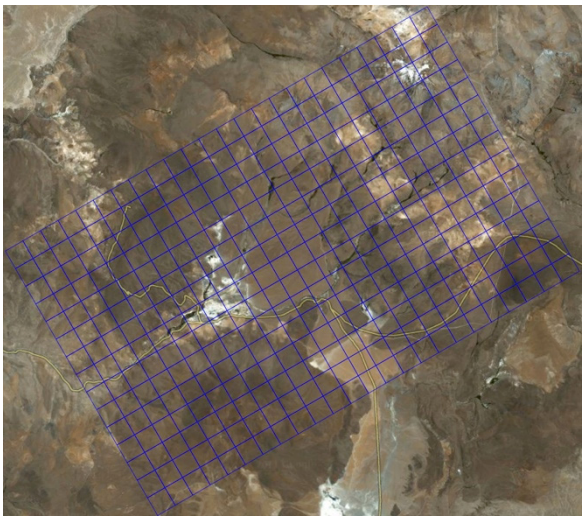

c)

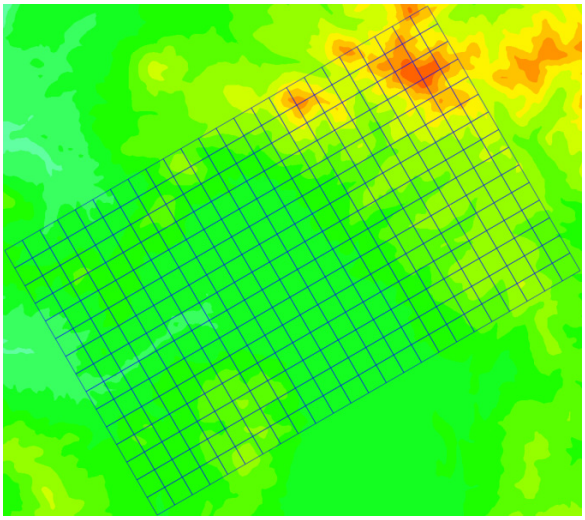

d)

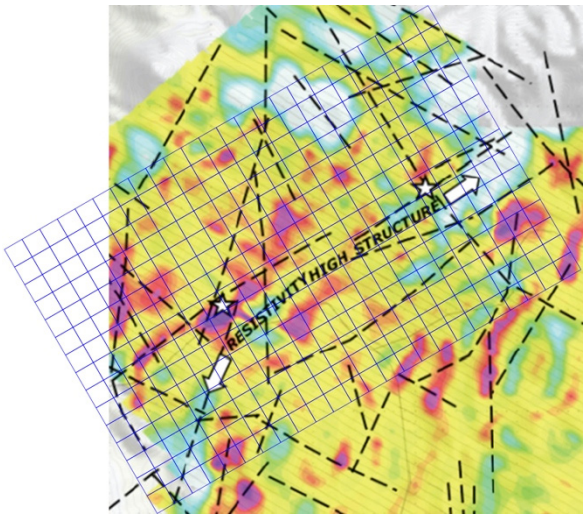

Figure 1: Model grid plotted with a) terrain contours, b) satellite image (Google maps), c) elevation and d) the ZTEM 2D resistivity at 500m depth (Legault *et al.*, 2012). In plot (a) line L1401 is indicated in green (-) and line L6000 in red (-). In plot (d) the locations of the Termas Lirima and Termas San Andres are indicated with stars.

a) b)

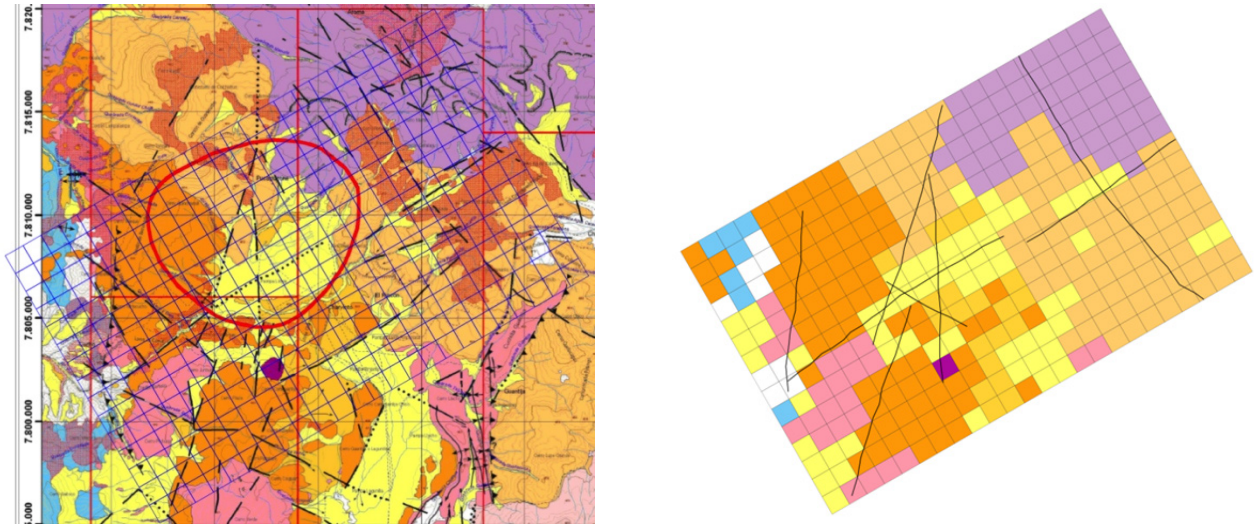

Figure 2: a) Model grid plotted with the surface geology (Arcos *et al*., 2011) and b) the surface geology in the model.

1.3 Geochemistry and isotopy in water samples.

The main discharges of hot springs are at the Termas Lirima and the Termas San Andres. The first is located in the SW corner of Pampa Lirima in the upper reaches of the Coscaya River, while the second is in the middle of the Andres-Jiguata valley, which is a tributary of the same river. Geologically, both seem to be interrelated through the same NE-SW alignment and their association with large areas of hydrothermal alteration of an argillic to advanced argillic steam-heated type (Arcos *et al*., 2011).

The Lirima hot springs are located in the lower part of the Lirima basin (approx. 4005 masl), flowing at temperatures between 38°C and 80°C, with chlorate sulfated-sodium chemical composition and electrical conductivitiy between 1300 and 1830 microS/cm. The chloride content varies between 250 and 310 mg /l, sulfate between 260 and 330 mg /l and pH levels between 6 and 7.

The San Andres hot springs discharge in the upper part of the basin (4380 masl). They have a sulphate calcium-sodium chemical signature, temperatures between 40°C and 60°C and an electrical conductivity between 1800 and 2140 microS/cm. The sulfate content varies between 670 and 700 mg/l, chloride between 130 and 141 mg/l and pH between 6 and 7 (Arcos *et al*., 2011). The δ34S values and δ18O of SO_4 indicate a source of SO_4 from Termas San Andres produced by oxidation of deep H_2S and possible dissolution of sulfates and sulfides. The $^{87}Sr/^{86}Sr$ ratio of the Termas San Andres waters may indicate an aquifer located in the lower levels of the late Miocene lavas that form the hills east of the basin. The $^{87}Sr/^{86}Sr$ ratio of the Termas Lirima waters can be correlated with the Lower to Middle Miocene volcanic rocks expected to occur deep in the basin. The δ2H and δ18O vs altitude relationship can be used to show a high altitude recharge for the thermal aquifers from above 4700 masl, and thus from the highest volcanic rock outcrops (Achurra, 2010).

Achurra (2010) proposed a conceptual hydrogeologic model that generates Na-Cl waters from a deep geothermal aquifer, which are mixed with an intermediate depth SO_4 water aquifer during upflow and subsequently discharge into the Termas Lirima. The waters that discharge into the Termas San Andres come from a peripheral steam heated shallow aquifer, containing SO_4 and acid water. The degassing from the same source that heats the geothermal aquifer of Termas Lirima is thought to be responsible for steam heated waters of the Termas San Andres.

2. MODEL SETUP

The objective of a numerical model is to represent the real system as accurately as possible so that the model may be used as a tool for understanding the behaviour of the system (O'Sullivan *et al.*, 2001). There are many considerations that impact the design of a model and the most important ones for the model presented in this work are described in the following sections.

2.1 Location, extent and orientation

The domain of the model must be large enough to include the important features of the geothermal system and positioned so that the lateral boundaries of the model do not have too large an effect on the model behaviour. In plot (b) of Figure 1 the surface expressions of the Pampa Lirima system can be seen to be in the central area of the model domain. Plot (a) presents the topography of the area overlaid by the model grid showing that model domain contains the entire Pampa Lirima basin. This ensures that the recharge for the system can be accurately represented. The ZTEM interpretation in plot (d) also shows that the low resistivity area is positioned in the centre of the model and also that the model grid is aligned with the main structure linking the Termas Lirima and Termas San Andres. This allows the option of assigning different permeabilities along the major structural system of the study area enabling it to be explicitly represented.

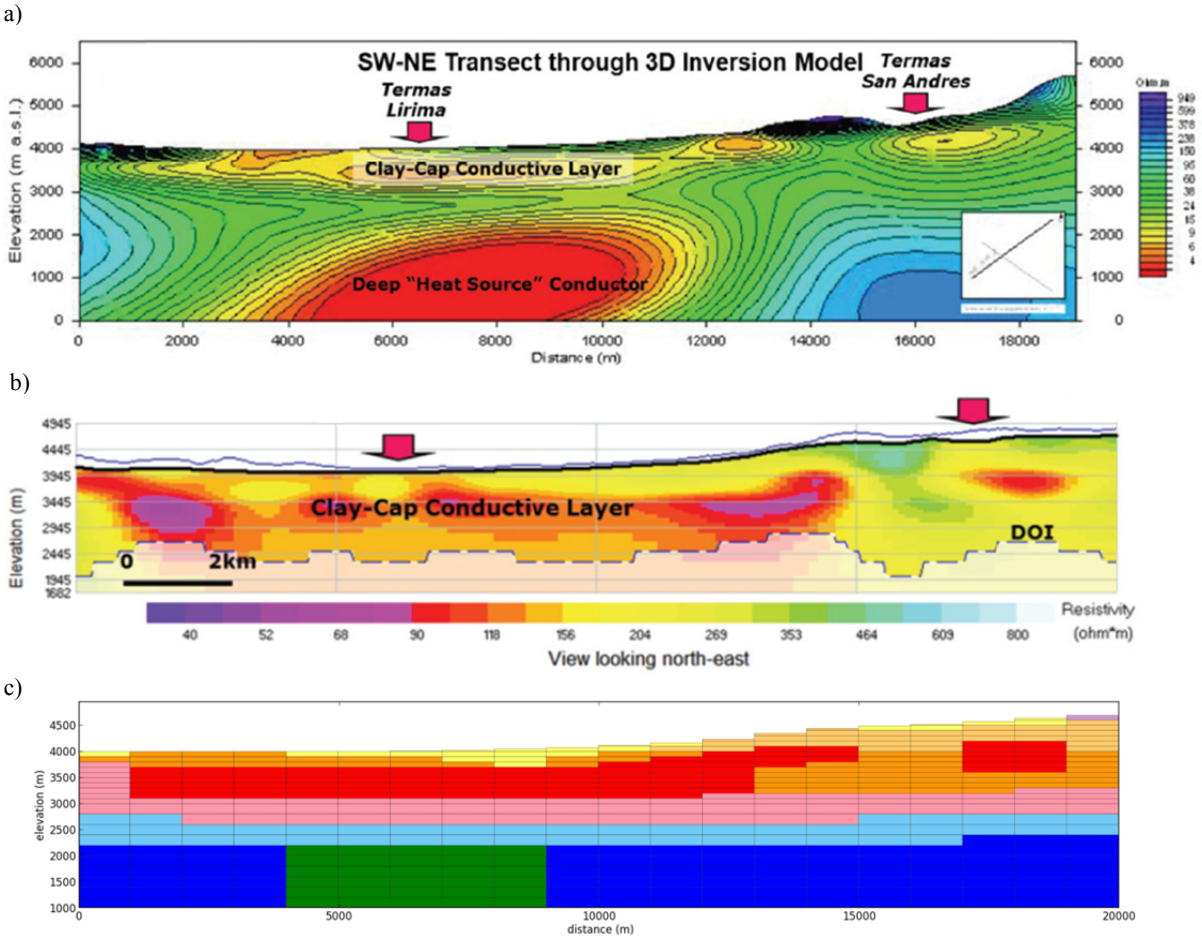

Figure 3: (a) MT and (b) ZTEM data (Legault *et al*., 2012) along line L6000 (Figure 1a) compared with (c) model geology.

Having positioned the model domain, the spatial discretisation must be determined. For this preliminary model the aim was to study the large-scale behaviour of the system and investigate the interaction between the two hot springs areas. Combined with the lack of detailed field data this meant that a relatively coarse mesh was used which allowed rapid model development. The details of the model domain are as follows:

Physical Dimensions	24 km x 15 km x 4.7 km
Model dimensions	24 x 15 x 37
Number of blocks	9169

Note that the model has 37 layers in the vertical direction. This was necessary in order to span the large range in topography, while also ensuring that the subsurface is accurately represented. The elevations of the area covered by the model range from ~4000 masl to 5700 masl, as is indicated in plot (c) of Figure 1. The implications of these extreme elevations are discussed in Section 2.4.

2.2 Model geology

The surface geology for the area has been described by Arcos *et al*. (2011) and is shown in Figure 2a.

Equivalent rock types were created in the model and assigned to the model blocks such that the surface geology was represented accurately. For the subsurface the different volcanic complexes were arranged so that they adhered to the conceptual model proposed by Arcos *et al*., 2011. Care was taken to ensure that the geological structures in the model were consistent with their position in the real system. For example Middle Miocene volcanic complex blocks are not found beneath Lower Miocene volcanic complex blocks, which in turn are not found beneath the Mesozoic Basement blocks. The resulting model structure can be seen in Figures 3c and 4c.

For the Quaternary and Plio-Pleistocene deposits the permeabilities were calculated from hydraulic conductivities given by Montgomery & Rosko (1996) of 4.8-9.2 x 10^{-3} cm/s. The permeabilities for the calibrated model are given for each rock-type in the Table 1.

The MT and ZTEM data shown in Figures 3 and 4 was also used to determine the position and size of the argillic clay-cap in the model. The model blocks that have been assigned the argillic clay-cap rock-type are shown in red in Figures 3c and 4c. The model blocks in the deep basement that correspond to the intersection of a structural system underneath the Termas Lirima have been coloured green in Figures 3c and 4c.

It is interesting to note that they correspond well with the deep conductor inferred from the MT results in Figures 3a and 4a. Finally note that the cross-sections in Figures 3c and 4c show how the surface of the model follows the topography.

a)

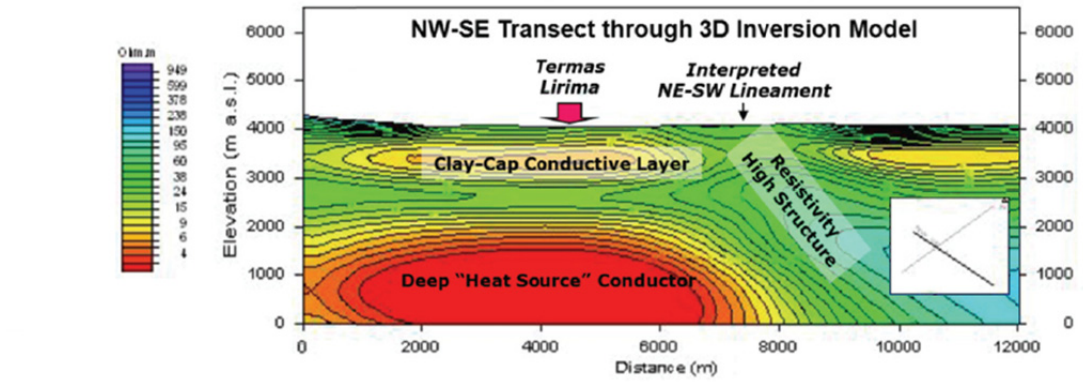

b)

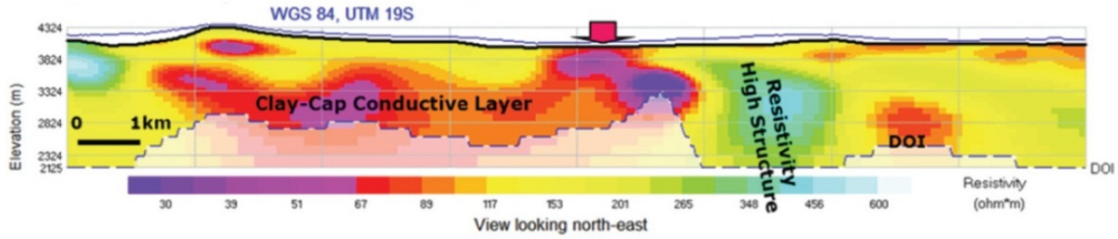

c)

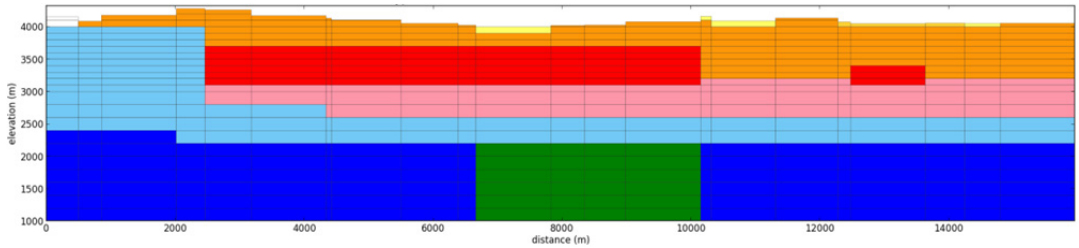

Figure 4: (a) MT and (b) ZTEM data (Legault *et al*., 2012) along line L1401 (Figure 1a) compared with (c) model geology.

Table 1: Rock-type specifications.

	Rock-type	Model Permeability		
		k x mD	k y mD	k z mD
	Quaternary Deposits	7500	7500	10
	Plio-Pleistocene Deposits	7500	7500	10
	Pliocene Volcanic Complexes	0.5	0.5	0.2
	Upper Miocene Volcanic Complexes	1	1	1
	Middle Miocene Volcanic Complexes	1	1	0.5
	Lower Miocene Volcanic Complexes	0.4	0.4	0.4
	Mesozoic Basement	0.2	0.2	0.2
	Miocene Porphyry	0.1	0.1	0.1
	Eocene Plutonics	0.1	0.1	0.1
	Argillic Clap-cap	0.1	0.1	0.1

2.3 Model structures

The main structures discussed in Section 1.2 are shown overlaid on the ZTEM 2D resistivity in Figure 1d and on the model surface geology in Figure 2b. Local geology shows a thrust system of reactivated, originally normal faults of a relatively high angle, however for the purposes of this preliminary model the structures were assumed to extend vertically downward to the bottom of the model without any dip. Within each rock formation new model rock-types were assigned to the blocks intersected by the structures. This approach allows the impact of the different stress states caused by the structures upon rock properties to be explicitly represented in the model.

Figure 5 shows the effect of this approach on the model structure in layer 29 at approximately 3000 masl. The layer consists of only two major formations; Lower Miocene Volcanic (LMV) complexes and Mesozoic Basement. However, once the major structures have been taken into account the LMV model rock type has been broken into eight different groups. Each of the new groups explicitly represents a major structure except for the Fractured and Andres groups which represent the intersections of multiple structures.

The table in Figure 5 also gives the calibrated permeabilities for each model rock-type. It can be seen that as expected the rock-types associated with the structure have significantly higher permeabilities. In the case of the Fracture group its horizontal permeability is 25 times higher than the basic formation group.

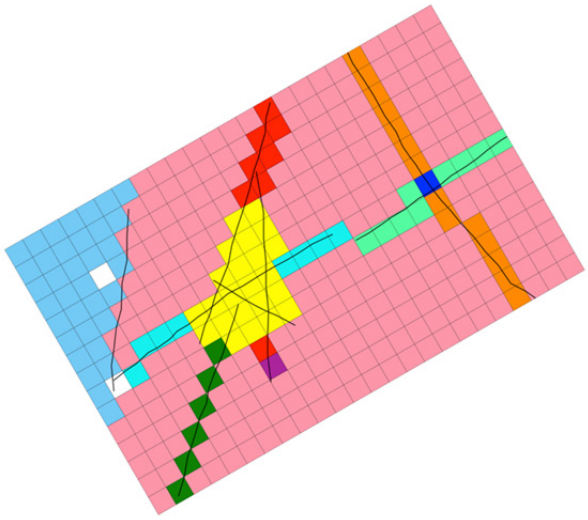

	Rock-type	Permeability		
		k x mD	k y mD	k z mD
	Lower Miocene Volcanic (LMV)	0.4	0.4	0.4
	LMV Fractured	10	10	1
	LMV Fault 1	0.8	0.4	1
	LMV Fault 2	0.8	0.4	2
	LMV Fault 3	0.4	0.4	1.5
	LMV Fault 4	0.8	0.8	1.5
	LMV Fault Andreas	0.4	0.4	10
	LMV Fault Lirima	0.4	0.4	1
	Miocene Porphyry	0.1	0.1	0.1
	Eocene Plutonics	0.1	0.1	0.1
	Mesozoic Basement	0.2	0.2	0.2

Figure 5: Structures represented in the model.

Also note that for groups Fault 1 and 2 the model rock-types have an enhanced permeability only along the fault and not across it, which is only possible due to the orientation of the model grid. The same method of representing structures was applied to each of the major formations in the model apart from the Quaternary and Plio-Pleistocene deposits which are already highly permeable and deemed to be unaffected by additional structural stresses

2.4 Boundary conditions

One of the objectives of the model design was to represent both the deep geothermal system and the shallow unsaturated zone above the water table. To achieve this the air/water equation of state EOS3 was used with a grid that followed the surface topography of the area. The boundary conditions at the top of the model were applied by creating atmosphere blocks of very large volume connected to the surface. The library toolbox PyTOUGH (Croucher, 2012) was used to calculate the pressure and temperature for each block based on the elevation of its centre and then to assign the values in the TOUGH2 initial condition file. Because the atmosphere blocks have a very large volume, their properties do not change throughout the simulation regardless of the conditions in the adjacent surface blocks (O'Sullivan *et al*., 2001).

The pressure p is calculated using Equation (1) (Wikipedia, 2013):

$$p = p_0 \left(1 - \frac{Lh}{T_0}\right)^{gM/RL}, \quad (1)$$

and the temperature T is given in Celsius using:

$$T = T_0 - Lh - 273.15, \quad (2)$$

where T_0 is the temperature at sea level in Kelvin, h is the altitude in meters and the constants are given in Table 2.

Table 2: Constants for calculation of high altitude temperature and pressure.

p_0	Pressure at sea level in Pa	101325
L	Temperature lapse rate K/m	0.0065
g	Gravity m/s^2	9.80665
M	Molar mass of dry air kg/mol	0.0289644
R	Universal gas constant J/(mol.K)	8.31447

The calculated temperature was bounded so that it is above 2°C as the standard TOUGH2 code is not designed to account for the effects of freezing. Given this approximation, the temperature varied from 2° to 5°C and the pressure from 0.52 to 0.64 bar. The atmosphere blocks were also set to contain a 0.9999 mass fraction of air.

Precipitation was approximated by injecting cold water into the surface blocks of the model. The rate of injection was based on an annual precipitation of 157 mm (Achurra, 2010) and an infiltration rate of 10% which is consistent with other numerical models (O'Sullivan et al., 2009). The water was injected at a temperature of 5°C corresponding to an enthalpy of 21.0 kJ/kg.

Note that the boundary conditions at the top of the model were held constant throughout the year. This assumption is known to be inaccurate given the highly seasonal weather conditions in the Pampa Lirima basin. The impact of seasonal variations in the top boundary condition on the deep geothermal reservoir is thought to be quite small but it is an area of ongoing research.

Because the model domain covers the entire Pampa Lirima basin, all of the meteoric recharge was accounted for. This allowed the use of closed lateral boundary conditions for the model. Any deeper, regional flows are not taken into account in the present model as their existence has not been confirmed or quantified.

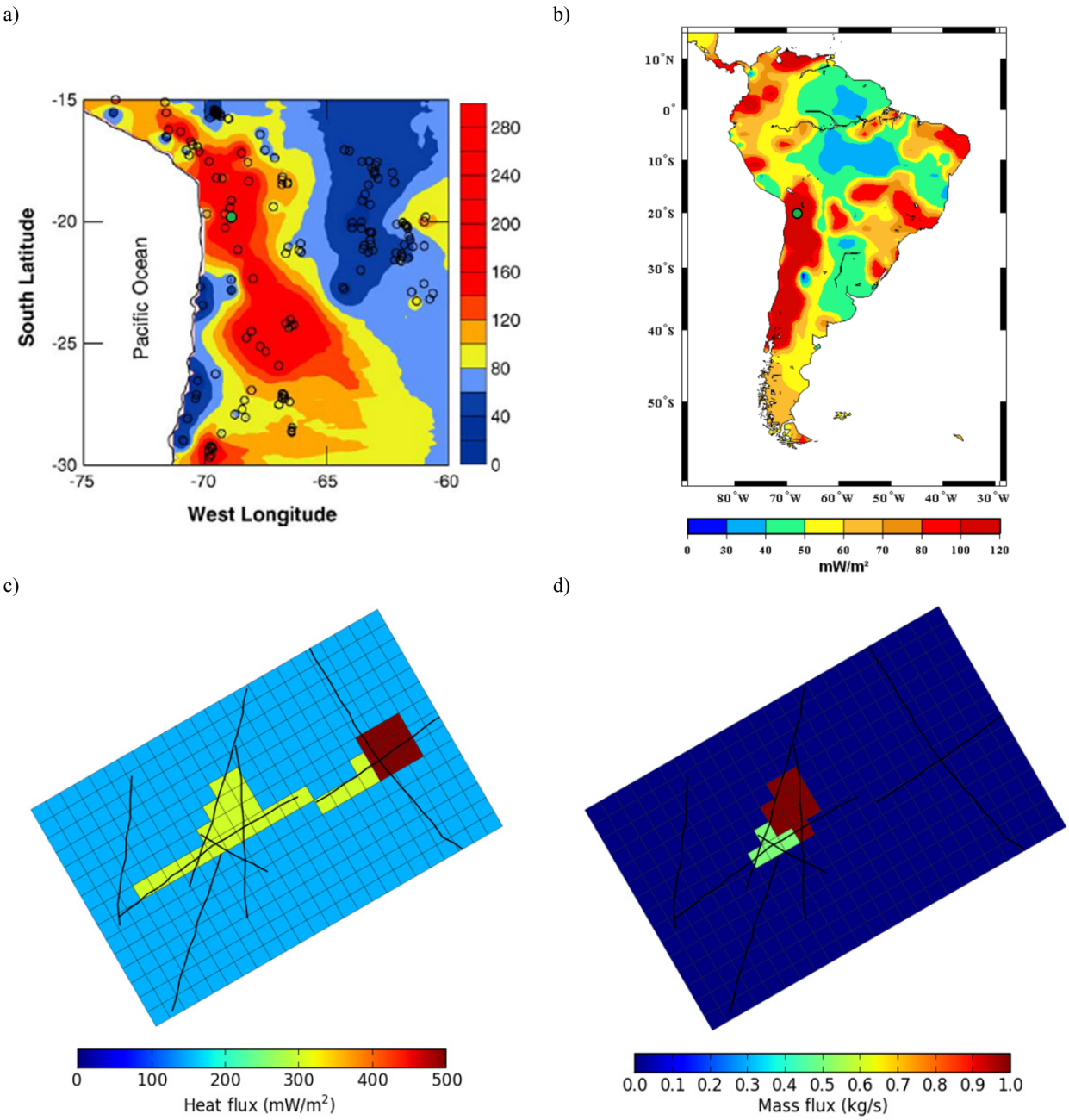

Figure 6: Regional heat flow maps from (a) Hamza et al. (2005) and (b) Cardoso et al. (2010). Location of Pampa Lirima basin indicated in green (•). Bottom boundary conditions for (c) the heat flux and (d) mass flux used in the model.

The boundary conditions at the bottom of the model were determined using information regarding the regional heat flux shown in Figures 6a and 6b (Hamza *et al.*, 2005; Cardoso *et al.*, 2010). For the blocks outside the upflow zones a heat flux of 150 mW/m^2 was applied as shown in Figure 6c. The heat flux applied along the structures and in the upflow zone was determined as part of the model calibration process and the results of the best-calibrated model are presented in Figure 6c.

It shows that a higher heat flux of 300 mW/m^2 was applied along the structure joining the two hot springs and throughout the region of intersecting faults under Termas Lirima. Under Termas San Andres an even greater heat flux of 500 mW/m^2 was applied.

The mass flux boundary conditions applied at the bottom of the model was also determined during the model calibration process discussed in the next section. The mass represents upflow into the model from parts of the geothermal system which are deeper than the bottom of the model domain.

The enthalpy of injected fluid was set 1290 kJ/kg, equivalent to a temperature of 290°C. This was based on the geothermometer estimates of 240°C given by Achurra (2010) for the main reservoir, 1000m shallower than the base of the model. Figure 6d shows that the base mass flux for the best-calibrated model is concentrated beneath the Termas Lirima, along the Lirima fault. The total mass injected is relatively small at 11 kg/s.

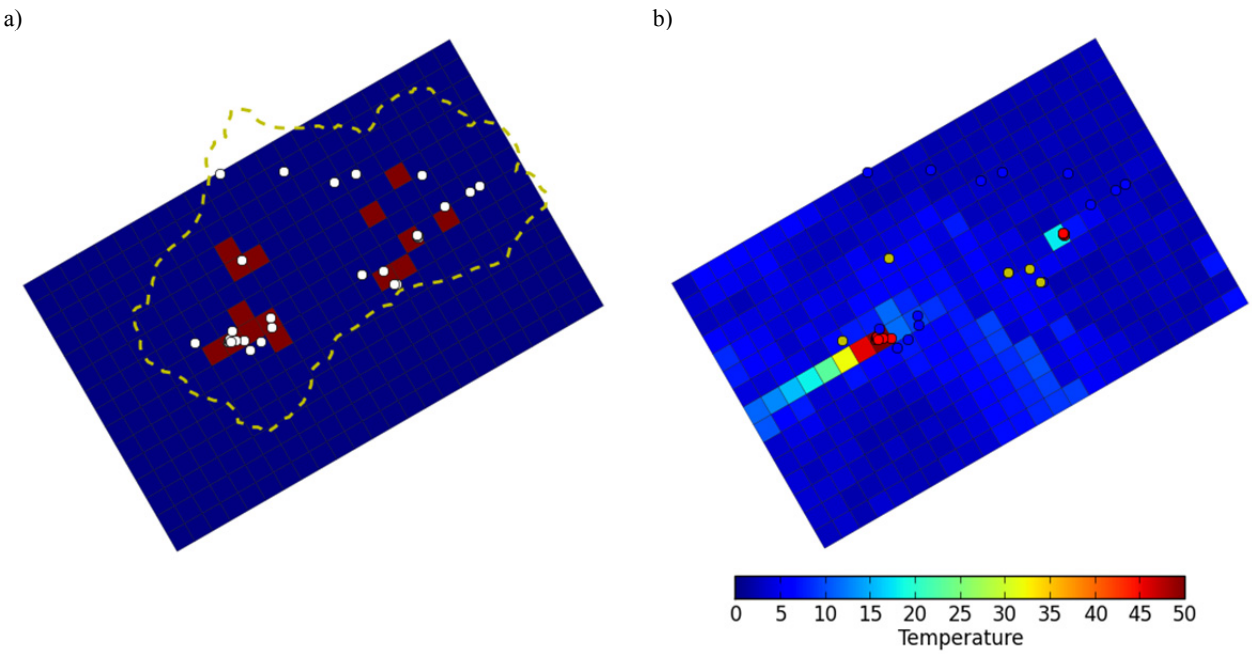

Figure 7: Results for: (a) mass flow and (b) temperature at the surface of the model. In plot (a) the observed springs are indicated as white circles (o), model columns with greater than 0.25 L/s mass outflow are indicated in red and the basin boundary is shown in yellow (-). In plot (b) the temperature of the springs are also indicated: hot (•), warm (•) and cold (•).

3. RESULTS

Once the model had been set up it was calibrated using all available field data for temperatures, flow rates and saturation. This was achieved by adjusting the permeabilities of the different model rock-types and the bottom boundary conditions, running the simulation and then comparing the results with field data. The process was repeated iteratively until a satisfactory match was achieved.

Without field data from wells the key information that was matched was the position and temperature of hot springs; the position of cold springs, the position of saturated ground (i.e. where the water table is at the surface) and the general reservoir temperature. Each of these is discussed in the following sections.

3.1 Surface features

The position of the water table is determined by the topography, the rate at which meteoric recharge occurs and the permeability of the near surface layers. The topography and the meteoric recharge are known but the shallow permeabilities must be calibrated using information regarding the water table level. The position of the water table can be determined using shallow wells and boreholes but in their absence it can be inferred from the position of saturated ground and springs.

The springs within the Pampa Lirima basin are shown as white circles in Figure 7a (Achurra, 2010). The only saturated ground in the basin also occurs at the locations of the hot springs as can be seen from the satellite images, similar to that shown in Figure 1b. The model permeabilities were adjusted until the position of the water table was matched well and the mass flux flowing out of the model into the atmosphere blocks matched estimates for the springs.

There is a good agreement between the model springs and the field data apart from in the north of the model where the topography is the highest and steepest. This discrepancy is a result of the model resolution which is very coarse (1km x 1km blocks) and the model is unable to represent the steep, mountain valleys where the upper springs appear. The coarse resolution has an overall smoothing effect which causes the spring either not to appear or to appear lower down the mountains, further to the south.

Data is not available for the exact flow rates of each of the springs but Achurra (2010) estimates the mass flow leaving the basin in the Coscaya River to be approximately 114 L/s. The combined total of the precipitation run-off and the mass flow from the springs in the best-calibrated model was 115.3 L/s. This close match indicates that the model is a good first approximation of the real system.

Figure 7b shows the good correlation between the temperatures measured in each of the springs and the temperatures estimated in the surface block of the best-calibrated model.

In general the model blocks are cooler which is to be expected because of the averaging effect of blocks 1 km^2 in area compared to the much smaller dimensions of individual springs.

This means that the model block corresponding to the Termas San Andres which has a temperature of 20°C can be interpreted as the average of a large area of dry ground at ~2°C and a small area of springs at the measured values of 40 to 60°C. The same is true of the blocks corresponding to the Termas Lirima and in both cases more accurate temperatures and heat fluxes can only be obtained with a significantly more refined model.

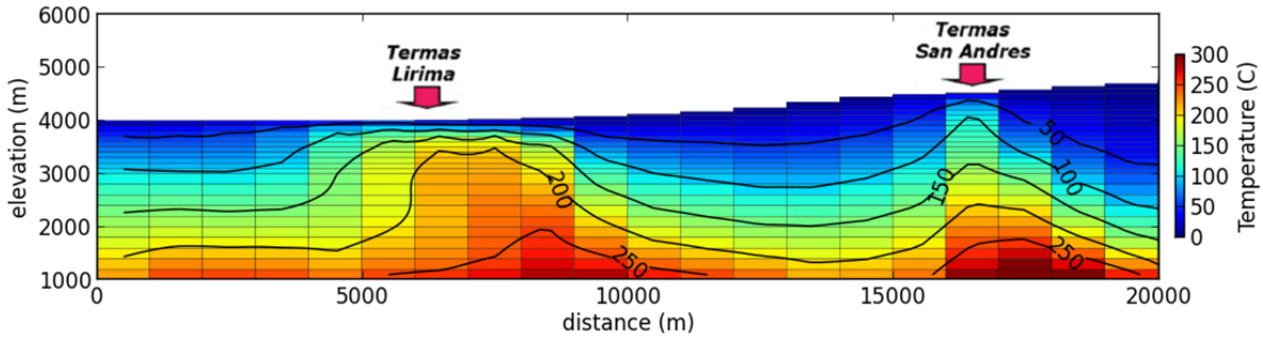

Figure 8: Model temperatures along the L6000 line (Figure 1a).

3.2 Temperatures

The temperature contours shown on the cross-section L6000 in Figure 8 demonstrate that the model predictions of the reservoir temperatures agree well with information from geothermometers. The model produces a relatively large, hot reservoir between 3000 and 2000 masl that is structurally controlled both in terms of the upflow mechanisms and the recharge. Figure 9 shows that at 3000 masl the model has a zone with temperatures greater than 180°C of approximately 9 km^2. It also shows clearly the structurally controlled cold recharge to both upflow zones.

Without more detailed subsurface measurements it is difficult to quantify the positions of the upflows but in this preliminary model the surface features have been matched well with two upflows that are distinct down to depths of 1000 masl. Below that level it appears likely that the systems are connected and in the model they are controlled by the same structure.

The model was not able to produce, nor rule out, the presence of a steam zone heating the meteoric recharge responsible or the Termas San Andres. This ambiguity is due to the coarse grid size of the model which can only resolve steam zones greater than 1k m x 1 km x 100 m. Future more refined models may be able to capture the steam zones that are thought to exist. However, the lack of a

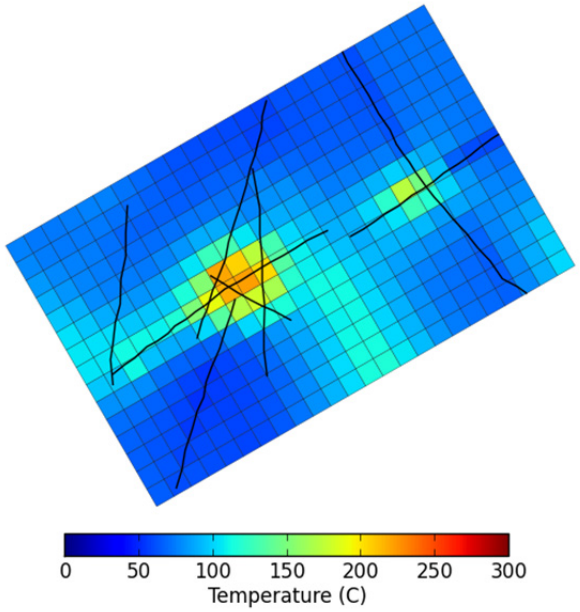

Figure 9: Model temperatures at 3000 masl.

steam zone in the model which estimates the surface and average reservoir temperatures quite well indicates that a large steam zone, greater than 1k m x 1 km x 100 m, is unlikely to exist.

4. CONCLUSION

The available geological, geophysical and geochemical data has been used to construct a conceptual model of the geothermal system in the Pampa Lirima basin in Northern Chile. This conceptual model has been used to develop a preliminary numerical model using the TOUGH2 simulator. The numerical model was calibrated using information from surface features, geology, geophysical observations, and geothermometers.

The model matches the observed data well despite its coarse resolution and provides a useful tool for understanding the behaviour of the natural system. The model indicates that the geothermal system has a relatively large reservoir with temperatures above 180°C which is structurally controlled.

The insights obtained in developing the model demonstrate the usefulness of numerical modelling of geothermal systems at an early stage, even prior to the availability of exploration well data. By increasing our understanding of a system, preliminary models may also be used to assist with the siting of exploration wells.

Once well data are available, the preliminary model could be refined and calibrated further making it a useful tool for investigating the future development of the system.

ACKNOWLEDGEMENTS

This research has been partially supported by FONDAP Centre of Excellence in Andean Geothermal N° 15090013. Thanks also to Mike O'Sullivan for his invaluable advice at various stages of this project.

REFERENCES

Achurra, L. (2010), "Estudio hidrogeoquímico sobre la interacción de aguas subterráneas profundas y someras en Pampa Lirima, Norte de Chile," Masters Thesis (Unpublished), UPC, Barcelona.

Arcos, R., Clavero, J., Giavelli, A., Simmons, S., Aguirre, I., Martini, S., Mayorga, C., Pineda, G., Parra, J., & Soffia, J. (2011), "Surface Exploration at Pampa Lirima Geothermal Project, Central Andes of Northern Chile," GRC Transactions, 35, 689-693.

Cardoso, R. R., Hamza, V. M., & Alfaro, C. (2010), "Geothermal resource base for South America: A continental perspective," proceedings World Geothermal Congress 2010, Bali, Indonesia, 25-29 April 2010.

Croucher, A. E. (2012), "PyTOUGH User's Guide," University of Auckland, Auckland, New Zealand, github.com/acroucher/PyTOUGH.

Hamza, V. M., Silva Dias, F. J. S., Gomes, A. J. L. & Delgadilho Terceros, Z. G., (2005), "Numerical and functional representations of regional heat flow in South America," *Physics of the Earth and Planetary Interiors* 152, 223–256.

Lahsen, A., Muñoz, N., & Parada, M. A., (2010), "Geothermal development in Chile," proceedings World Geothermal Congress 2010, Bali, Indonesia, 25-29 April 2010.

Legault, J., Lombardo, S., Zhao, S., Clavero, J., Aguirre, I.,Arcos, R., & Martinez, E. (2012), "ZTEM airborne AFMAG EM and ground geophysical survey comparisons over the Pampa Lirima geothermal field in northern Chile," Report, Geotech.

Montgomery, E., & Rosko, M. (1996), "Groundwater exploration and wellfield development in the Pampa Lagunillas and Pampa Lirima areas, Provincia de Iquique, Chile," Revista Geologica de Chile 23(2), 135-149.

O'Sullivan, M. J., Pruess, K., & Lippmann, M. J. (2001), "State of the art of geothermal reservoir simulation," Geothermics, 30(4), 395-429.

O'Sullivan, M. J., Yeh, A., & Mannington, W. I. (2009), "A history of numerical modeling of the Wairakei geothermal field," *Geothermics*, 38, 155-168.

Tassi, F., Aguilera, F., Darrah, T., Vasseli, O., Capaccioni, B., Poreda, R. & Delgado Huertas, A. (2010), "Fluid Geochemistry of hydrothermal systems in the Arica-Parinacota, Tarapacá and Antofagasta regions (Northern Chile)," *Journal of Volcanology and Geothermal Research*, Vol. 192, p. 1-15.

Wikipedia contributors (2013), "Atmospheric pressure." Wikipedia, The Free Encyclopedia. Wikipedia, The Free Encyclopedia, Web.